Journal of
Synchrotron Radiation

ISSN 0909-0495

Received 22 March 2010
Accepted 16 July 2010

A new technique to examine individual pollutant particle and fibre deposition and transit behaviour in live mouse trachea

Martin Donnelley,[a]* Karen K. W. Siu,[b,c] Kaye S. Morgan,[c] William Skinner,[d] Yoshio Suzuki,[e] Akihisa Takeuchi,[e] Kentaro Uesugi,[e] Naoto Yagi[e] and David W. Parsons[a,f,g,h]

[a]Respiratory and Sleep Medicine, Women's and Children's Hospital, Adelaide, Australia, [b]Monash Centre for Synchrotron Science, Monash University, Victoria, Australia, [c]School of Physics, Monash University, Victoria, Australia, [d]Ian Wark Research Institute, ARC Special Research Centre for Particle and Material Interfaces, University of South Australia, Australia, [e]SPring-8/JASRI, Hyogo, Japan, [f]Centre for Stem Cell Research, University of Adelaide, Australia, [g]Department of Paediatrics and Reproductive Health, University of Adelaide, Australia, and [h]Women's and Children's Health Research Institute, Adelaide, Australia. E-mail: martin.donnelley@adelaide.edu.au

During respiration, particles suspended in the air are inhaled and unless cleared by airway defences they can remain and affect lung health. Their size precludes the use of standard imaging modalities so we have developed synchrotron phase-contrast X-ray imaging (PCXI) methods to non-invasively monitor the behaviour of individual particles in live mouse airways. In this study we used these techniques to examine post-deposition particle behaviour in the trachea. PCXI was used to monitor the deposition and subsequent behaviour of particles of quarry dust and lead ore; fibres of asbestos and fibreglass; and hollow glass micro-spheres. Visibility was examined *in vitro* and *ex vivo* to avoid the complicating effects of surrounding tissue and respiratory or cardiac motion. Particle behaviour was then examined after deposition onto the tracheal airway surfaces of live mice. Each particle and fibre looked and behaved differently on the airway surface. Particles lodged on the airway shortly after deposition, and the rate at which this occurred was dependent on the particle type and size. After the live-imaging experiments, excised airway samples were examined using light and electron microscopy. Evidence of particle capture into the airway surface fluids and the epithelial cell layer was found. PCXI is a valuable tool for examining post-deposition particulate behaviour in the tracheal airway. These first indications that the interaction between airways and individual particles may depend on the particle type and size should provide a novel approach to studying the early effects of respired particles on airway health.

Keywords: particles; pollution; airway surface; lung; trachea; mucociliary transit; non-invasive; X-ray imaging; mouse.

1. Introduction and objectives

Air pollution is a significant environmental and health concern. Man-made airborne pollutants from a wide variety of sources are suspended in the air in liquid, gaseous or solid forms. We have previously described a new technique to image solid particulates and fibres such as quarry dust, fibreglass, asbestos and lead in mouse nasal airways (Donnelley *et al.*, 2009). These pollutants have the potential to produce deleterious acute or delayed health effects, and can impact on asthma, cystic fibrosis (CF), bronchitis, emphysema, respiratory allergies and heart disease (O'Connor *et al.*, 2008). For example, CF patients living in regions with high particulate matter air pollution, such as in metropolitan areas, have decreased lung function as well as an increased risk of pulmonary exacerbations (Goss *et al.*, 2004). Particulate pollution can affect young children more severely than adults, owing to their different lung size and physiology, breathing patterns and rapid development (Wildhaber, 2006). The manner in which particulates deposit onto the airway surface and their behaviour after deposition are poorly understood but are likely to influence or predict key aspects of their subsequent pathophysiology.

Mucociliary transit (MCT) function is one measure of the likely effectiveness by which the airways clear inhaled pollutant particles and is a diagnostic indicator of airway health. To

help determine the effectiveness of genetic (Stocker *et al.*, 2009; Limberis *et al.*, 2002) and other potential therapeutics for CF airway disease we have developed novel MCT monitoring methods, based on measuring the transit rate of individual deposited particles, that can be used *in vivo* in mice. Existing methods for quantifying bulk particle clearance in airways (Grubb *et al.*, 2004; Donaldson *et al.*, 2007; Livraghi & Randell, 2007) are unable to non-invasively detect and track the motion of individual pollutant particles in real time and with high resolution. Direct non-invasive visualization of the behaviour of deposited particles in animal-model airways is expected to improve our understanding of airway surface function and suggest novel methods for prevention or treatment of respiratory disease in both young children and adults.

This study utilized synchrotron phase-contrast X-ray imaging (PCXI) to detect, monitor and compare the deposition and transit behaviour of selected pollutant particles in the tracheal airway in live mice. PCXI provides enhanced image contrast by utilizing X-ray refraction in addition to conventional absorption and is particularly useful for achieving soft tissue contrast where the absorption differences are small. Tissue boundaries are enhanced by the phase changes induced by differences in their X-ray refractive indices, provided the X-ray beam has sufficient spatial coherence and the sample-to-detector distance is sufficiently long (Snigirev *et al.*, 1995; Cloetens *et al.*, 1996; Wilkins *et al.*, 1996), characteristics that are achievable using a synchrotron source. We have demonstrated the use of PCXI for novel non-invasive airspace imaging in small animals (Parsons *et al.*, 2008), and for non-invasive particulate detection in live mouse *nasal* airways (Donnelley *et al.*, 2009; Siu *et al.*, 2008). Since deleterious respiratory health effects are predominantly lung-based, the objective of the current study was to establish PCXI techniques to examine particulate deposition and transit behaviour in live mouse trachea. Using commonly inhaled pollutants delivered within a saline carrier we sought to document particle and fibre visibility, post-deposition behaviour on the *tracheal* airway surface, transit rates, differences between particle and fibre types, histological effects and radiation dose. We also aimed to determine whether the anatomical and physiological differences between the *nasal* and *tracheal* airways resulted in different post-deposition behaviour to that which we previously recorded in the mouse nose.

2. Methods

Experiments were performed on the BL20XU undulator beamline at the SPring-8 synchrotron radiation facility in Japan, under approvals from the Animal Ethics Committee of SPring-8, and of the Children, Youth and Women's Health Service, Adelaide. The imaging hutch was located in the Biomedical Imaging Centre, 245 m from the storage ring, and the imaging layout (see Fig. 1) was as shown previously (Parsons *et al.*, 2008). Monochromatic 25 keV (λ = 0.5 Å) X-rays were selected using a standard double-crystal monochromator (Yabashi *et al.*, 1999). At the imaging station the beam size was approximately 4 mm (H) × 2 mm (V). A

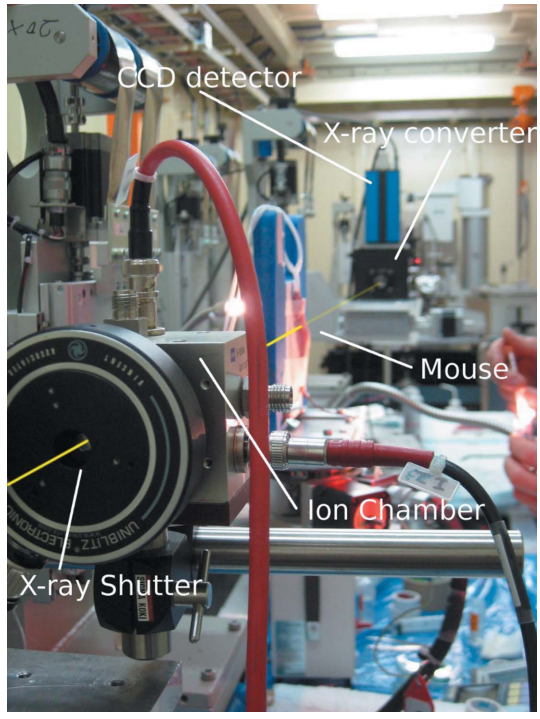

Figure 1
The *in vivo* imaging set-up in the BL20XU imaging hutch with the approximate path of the X-ray beam shown in yellow. A diagram of the set-up was shown previously by Parsons *et al.* (2008). The X-ray beam passed through a shutter, ion chamber and the mouse trachea before reaching the X-ray converter and camera. The propagation distance between the mouse and X-ray converter was 135 cm. The hand of a researcher is visible on the right, preparing to deliver a particulate sample to the mouse trachea.

propagation (sample-to-detector) distance of 135 cm was chosen to produce a sufficiently strong bright/dark fringe from the boundary of each particle, so that they could be identified amid intensity variations introduced by overlying tissue and skin. Images were captured using a high-resolution X-ray converter (AA50 Hamamatsu Photonics) with a charge-coupled device (CCD) detector. The converter used a 10 µm-thick scintillator (Lu_2SiO_5:Ce) to convert X-rays to visible light, which was then directed to the CCD using a ×20 microscope objective lens with a numerical aperture of 0.4. The CCD detector was a pco.4000 (PCO Imaging) with an array size of 4008 × 2672 pixels and a 9 µm × 9 µm native pixel size. This set-up resulted in an effective isotropic pixel size of 0.45 µm and a field of view of 1.8 mm × 1.2 mm. The beam was limited to approximately this size using slits where the beam enters the experimental hutch to reduce the radiation dose to the animals. The FWHM of the point spread function, as determined from a horizontal edge image, was measured at 3.6 µm. A fast shutter (Uniblitz XRS6 with VMM-T1 timer unit) received triggers from the ventilator (refer to the *in vivo* study description below) to control image capture to minimize the dose between exposures. Exposure times of 100 ms, 180 ms and 280 ms were used for the *in vitro*, *ex vivo* and *in vivo* studies, respectively. These exposure lengths produced the optimum images, capturing sufficient incident photons to fill the potential dynamic range (2^{14} grey

levels) of the detector, providing the maximal signal-to-noise ratio without inducing detector saturation.

2.1. *In vitro* studies

In this experiment the same five raw pollutant samples previously tested in the mouse *nasal* airway (Donnelley *et al.*, 2009) were examined *in vitro* to verify the particle visibility under PCXI, the particle size distribution, and to determine a suitable concentration for *in vivo* testing in the *trachea*. Chrysotile (white asbestos), provided by the South Australian Museum, was manually ground under water and allowed to settle to produce fibre fractions suitable for examination. Fibreglass from a commercial pipe insulation, and galena, the natural mineral form of lead sulfide (PbS) in lead ore, from the South Australian Museum, were both finely ground using a mortar and pestle. Dolomite quarry dust that settled out of airborne suspension was provided courtesy of the Boral Resources (SA) Limited Linwood Quarry (Adelaide, South Australia). Hollow silver-coated glass beads with a median diameter of 14 µm were obtained from Potter Industries (Melbourne, Australia) for use as reference particles of known composition, shape and size.

For the *in vitro* study raw samples were prepared in physiological saline at concentrations of 0.1% *w*/*v* and 1% *w*/*v*, and 15 µl samples were pipetted inside small steel washers (7/32" inside diameter) pressed onto the adhesive surface of Kapton tape, a polyimide film highly transparent to X-rays (Argon Masking, PC500, ∼25 µm thick with ∼38 µm-thick silicon adhesive). The washers containing the samples were then sealed using a second piece of tape (test samples are shown in Fig. 2*f*) and mounted for imaging within the imaging hutch on a motorized sample stage with *x* and *y* translation (in a plane perpendicular to the beam direction).

The *in vivo* PCXI images of the pollutants were analysed using *Matlab* (version 7.9.0 R2009b, The MathWorks) to determine their size distribution. Images were automatically adjusted using adaptive histogram equalization, a threshold applied to binarize the image, and a connectivity analysis performed to identify unique objects. The effective diameter of the particles as well as the length and width of the fibres were then calculated using the known effective pixel resolution of the image to produce a distribution histogram. Only objects with a size greater than 4 µm were included because smaller fragments could not be accurately separated by this analysis.

2.2. *Ex vivo* studies

A pilot *ex vivo* experiment was performed using one HOS:HR-1 mouse humanely killed by Nembutal overdose (∼325 mg kg^{-1} i.p.). The trachea was excised and placed into a sealed and humidified study chamber with Kapton film windows to minimize specimen dehydration during the experiment. The chamber held the excised trachea vertically with each end cannulated with 20 Ga i.v. catheters (Insyte, Becton Dickinson, Utah, USA). The chamber was mounted on the sample stage in the imaging hutch such that the X-ray beam passed laterally through the excised trachea in the same orientation used in subsequent *in vivo* studies. Images were captured at baseline and after delivery of 15 µl bolus samples of the particulates suspended in 0.9% saline. After treatment the sample chamber was also translated vertically to allow the full length of the excised trachea to be imaged using a number of exposures (see Fig. 4*a*).

2.3. *In vivo* studies

In vivo experiments were performed using 15 hairless HOS:HR-1 mice weighing ∼18–26 g. This hairless strain, commonly used for dermatological experiments in Japan, was chosen to eliminate interference from fur in the high-resolution PCXI images. Mice were anaesthetized with Nembutal (∼72 mg kg^{-1}, i.p.) and the imaging area around the trachea was cleared of residual fur using depilatory cream (Nair, Church & Dwight, Australia). The mice were then intubated using an arterial guide wire and a 20 Ga i.v. catheter as an endotracheal (ET) tube (Hamacher *et al.*, 2008). The ET tube was inserted into the trachea to a fixed depth of 22.5 mm from the nose tip to avoid physical perturbation of the more distal imaging region. The catheter needle-hub was immediately cut off to minimize respiratory dead-space, and so that the ET tube was ready for connection to the ventilator circuit. Mice were secured to a polyethylene imaging board with their dorsal incisors hooked over a stainless-steel wire loop and the limbs, shoulders and torso taped to the board to minimize body movements that interfere with high-resolution imaging.

The imaging board was mounted on the hutch sample stage such that the X-ray beam passed laterally through the mouse trachea, at approximately three cartilage rings below the tip of the ET tube (see Figs. 1 and 4*b*). The ET tube was connected to a flexiVent small animal ventilator (Scireq, Canada), and anaesthesia was maintained using a passively humidified isoflurane O_2 mixture [Fisher and Paykel HC100 respiratory humidifier and Univentor U400 (Zejtun, Malta) isoflurane vaporiser]. Ventilation was set at 80 breaths per minute, a tidal volume of 20 ml kg^{-1} (minute ventilation of approximately 1.6 ml g^{-1}), and ∼3 cm H_2O of PEEP. The almost continuous motion present during normal breathing provides a technically challenging experimental setting so the ventilatory profile was configured with $T_{\rm inspiration}$ = 0.1875 s, $T_{\rm pause}$ = 0.3125 s and $T_{\rm expiration}$ = 0.25 s, providing a sufficient end-inspiratory pause to allow relatively motion-artefact-free image capture.

Groups of three mice were exposed to each of the five particulates. Image capture was triggered by the ventilator once every 14 breaths (10.5 s). After 3.5 min of baseline collection (20 images) a 15 µl sample of the particulate suspended in saline was manually delivered in a single bolus over 10 s *via* the ET tube using a 25 µl glass syringe. This involved opening the hutch door, manually disconnecting and reconnecting the ET tube from the ventilator and closing the hutch door, producing a delay of typically 1 min between particulate delivery and imaging. Image acquisition was resumed at the same rate for a further 42 min (∼240 images), creating a dataset consisting of 260 images per mouse. Since

these mice were not allowed to recover after completion of the experiment we did not attempt to minimize the delivered radiation dose (beyond using slits to reduce the beam size and a fast shutter to minimize exposure to the beam); rather, we maximized both the number and quality of the images acquired to ensure the best possible experimental results.

2.4. Post-experimental analyses

Mice were humanely killed *via* Nembutal overdose without loss of anaesthesia. In some animals the trachea was excised and fixed for at least 1 h in a non-aqueous fixative (perfluorocarbon FC-72, 3M Corporation, containing 1% osmium tetroxide, OsO_4) to preserve surface fluid, secretions and mucous *in situ* for subsequent light and electron microscopy to determine where particulates lodged after deposition (Sims *et al.*, 1991). The fixed samples were transferred to 70% ethanol, embedded in acrylic resin and sectioned for light microscopy (post-stained with toluidine-blue) and transmission electron microscopy (post-stained with a saturated solution of ~4% uranyl acetate followed by lead citrate). The elemental composition of the particulates in the fixed tracheal sections was also verified under transmission electron microscopy (TEM) using energy-dispersive X-ray spectroscopy (EDS) microanalysis (Philips CM-200) of unstained sections. Control samples of the raw test particulates were also embedded in resin to provide EDS reference spectra with which the results were compared.

The mouse anatomy at the imaging location introduced confusing detail into the PCXI images since other structures in the path of the X-ray beam, such as rings of tracheal cartilage, skin, bone and other tissues, could obscure individual small particles in single images. To facilitate rapid and accurate location of relevant particles, each image sequence was flat/dark-corrected and contrast enhanced (*Matlab*), and analysed with simple motion-detection software (VirtualDub, version 1.8.6, Avery Lee, using the MSU Motion Estimation plug-in, Graphics and Media Lab, Moscow State University) to reveal where motion was occurring by applying digital image subtraction and filtering algorithms that identify regions of the image that change between frames (Donnelley *et al.*, 2009). For high-quality motion detection the background must remain still compared with the moving objects to be detected, hence special efforts were made to minimize the movement of the mouse during imaging, including the use of restraining boards and respiratory-gating as described above. Particle transit rates were calculated by manually tracking the motion of an individual particle through the image sequence, measuring the distance it travelled using the known effective pixel resolution of the image and then dividing by the elapsed time between the frames.

3. Results

3.1. *In vitro* studies

The *in vitro* PCXI visibility of the pollutant particles in saline was similar to that previously reported for samples mixed in distilled water (Donnelley *et al.*, 2009). Owing to the relatively long propagation distance many particles were visible owing to phase or absorption contrast, or a combination of both. Fig. 2 shows the results from these *in vitro* studies, and clearly demonstrates the differences in appearance between particle types. The samples were visible both dry and within saline, indicating that saline had little effect on the overall contrast. For example, absorption dominated the image contrast for galena, and produced shadows with few fringes (Fig. 2*d*). By comparison, hollow glass beads strongly refracted the X-rays and produced phase contrast visible as light and dark fringes; however, no dark shadows were produced since the beads are very thin walled and hollow (Fig. 2*e*). Other particles, such as quarry dust, showed both phase and absorption contrast, appearing darker where the object attenuated the beam, as well as displaying bright/dark fringes around the particle edges (Fig. 2*b*).

Based on our *in vitro* observations a concentration of 1% *w*/*v* was selected for the *ex vivo* and *in vivo* studies to ensure sufficient particulates were present in a 15 µl sample to potentially be visible when deposited into the mouse trachea. The manual grinding employed during the particulate preparation was clearly effective as few large particulates were present, excluding some long asbestos and fibreglass fibres. As

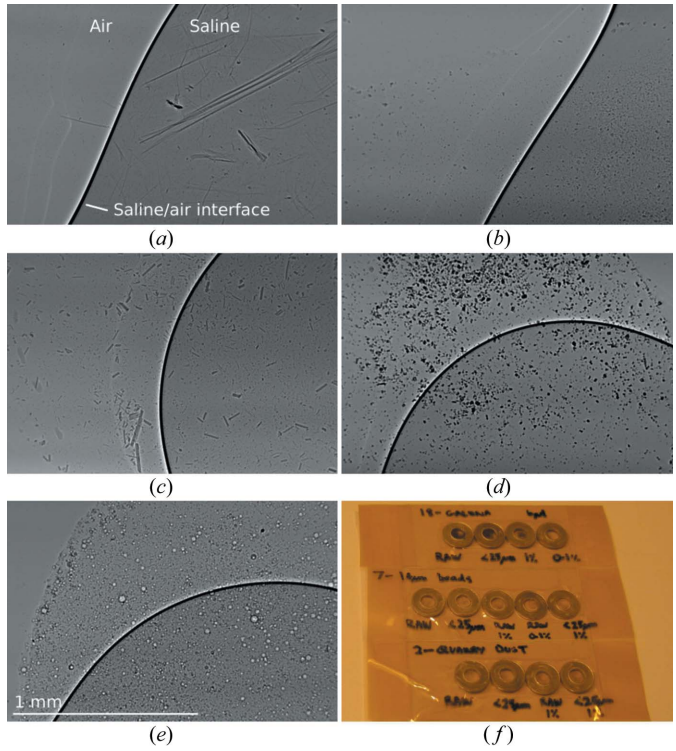

Figure 2
PCXI images (1.8 mm × 1.2 mm) of 15 µl samples of 1% *w*/*v* particulates suspended in saline used for the *in vivo* study are shown for (*a*) asbestos, (*b*) quarry dust, (*c*) fibreglass, (*d*) galena and (*e*) silver-coated hollow glass beads. All images are arranged so that the particulates can be seen wet and dry. The dry particles are on the top/left, and the particles in saline are present in the bottom/right. The test sample set-up is shown in (*f*); samples were placed in the centre of small washers that were encapsulated in Kapton tape.

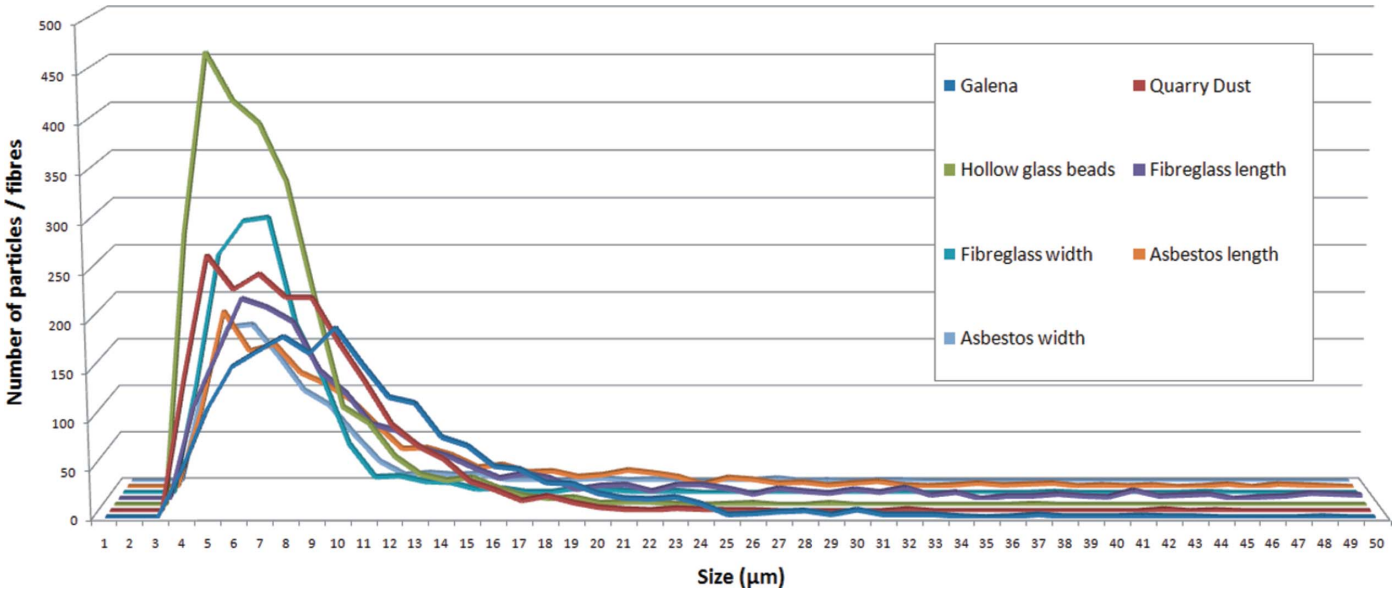

Figure 3
Particle and fibre size distribution measured from the *in vivo* images in Fig. 2.

previously reported (Donnelley *et al.*, 2009), the asbestos could not be finely ground so we relied on differential settling in water to obtain finer size fractions. The size distribution of the particles and fibres is shown in Fig. 3, and verifies that particles typically ranged in diameter from 5 µm up to 12 µm with a small number of larger particles present. The width of the fibres was also within this range, but the lengths were significantly greater. Fibreglass fibres of length $\geq$40 µm were not uncommon, but only the asbestos fibres were longer than 50 µm. Despite a stated manufacturers nominal diameter of 14 µm, the majority of the glass beads were smaller.

3.2. *Ex-vivo* studies

Prior to use in live mice, particle visibility was verified in a segment of excised mouse trachea. All particulates were easily detected and had similar appearances to those observed in the *in vitro* study [all particulates are visible in Fig. 4(*a*)]. Although all particulates were detectable, the quarry dust particles were more difficult to detect than the fibreglass, galena and the hollow glass beads. In addition, only one bundle of asbestos fibres was visible in the trachea in contrast to the other particulates, of which many individual particles could be detected. Despite using an enclosed chamber we did find that the excised trachea tended to rapidly and visibly dehydrate resulting in noticeable shrinkage even over a 10 min imaging period. Since the airway tissue was grossly affected by this process we did not attempt to use this system to analyse post-deposition behaviour.

3.3. *In vivo* studies

3.3.1. Site of particulate delivery in mouse airway. We found that inserting the ET tube to a depth of 22.5 mm placed the ET catheter tip two to three cartilage rings below the top of the trachea (Fig. 4*b*). In most cases the imaging region was

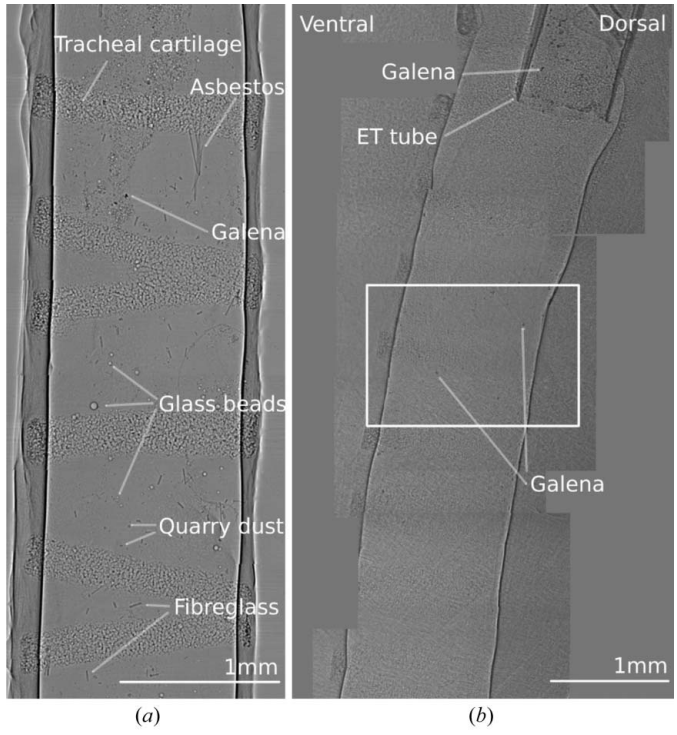

(*a*) (*b*)

Figure 4
(*a*) A montage of nine individual PCXI images from the pilot *ex vivo* experiment that examined an excised mouse trachea. The images were taken after all five particulates had been delivered within individual 15 µl boluses. All five particle types are clearly visible and marked. (*b*) An *in vivo* montage of 15 individual PCXI images with the ET tube uppermost in the trachea. The ET tube opening is approximately two cartilage rings from the top, and the standard imaging location, usually three rings below the bottom of the ET tube, is marked with a white rectangle. Dark particles of galena are apparent within the ET tube as well as at the imaging site in the trachea. Image alignment is poor at some montage frame edges owing to respiratory movements that occurred between image captures.

three cartilage rings (~1.5–2 mm) below the end of the ET tube, but in some mice this was adjusted slightly to ensure a clear and less obstructed view of the trachea.

3.3.2. Imaging set-up and particulate delivery effects. The 15 µl dose provided sufficient visible fluid and particulates to be monitored in the trachea and induced no noticeable change in respiratory effort or frequency, as measured by monitoring the airway pressure recorded by the flexiVent. In earlier pilot studies higher doses induced transient coughing that produced blurred images. We noted that for the first 30 min of the experiment image quality was excellent, due largely to the respiratory-gating. It is important to note that the gating only minimized intra-frame motion. Some inter-frame motion still made isolating particle-motion difficult, although securely taping the body to the restraint board minimized this effect. After approximately 30 min most mice displayed large irregular respiratory excursions initially every ~10 breaths, increasing in frequency and magnitude as the experiment continued. Mice remained deeply anaesthetized as assessed by foot pinch, but these movements eventually degraded the quality of the images because the end-inspiratory breath holds became ineffective. Independently increasing the level of anaesthesia (*e.g.* isoflurane to 3.5%) as well as the tidal volume (to 25 ml kg^{-1}), or using a single total lung capacity manoeuvre once every 5 min to ensure complete lung filling did not alter these complicating respiratory effects.

One mouse was imaged in a supine position and this almost eliminated the irregular respiratory movements, suggesting that the head-high mounting was a likely cause of the respiratory instability we observed. Consistent with this was the observation that the tracheal diameter of some mice reduced over the extended imaging periods, in one case by up to ~0.2 mm. The abdominal contents in some mice also slumped substantially by the end of the imaging period, and cartilage rings moved down slowly relative to the X-ray beam, in some cases by up to ~0.2 mm, such that the imaging position appeared to change over time.

During these experiments the incident photon flux was approximately 7.47×10^9 photons s^{-1}, producing an estimated dose of approximately 0.13 Gy per exposure delivered to the 1.8 mm × 1.2 mm imaging area for each of the 280 ms exposures used *in vivo*.

3.3.3. Appearance and behaviour of particulates in live mouse trachea. The presence and behaviour of fibreglass, galena, quarry dust and the hollow silver-coated glass beads could be detected *in vivo*, with visibility improved by using motion-detection software during post-experimental processing. Of the pollutants that we could detect with PCXI, galena was the most visible and quarry dust the least visible. Fibreglass and the hollow silver-coated glass beads provided intermediate visibility. Despite analysing both the raw and motion-detected images we did not positively identify asbestos fibres in any of the image sequences.

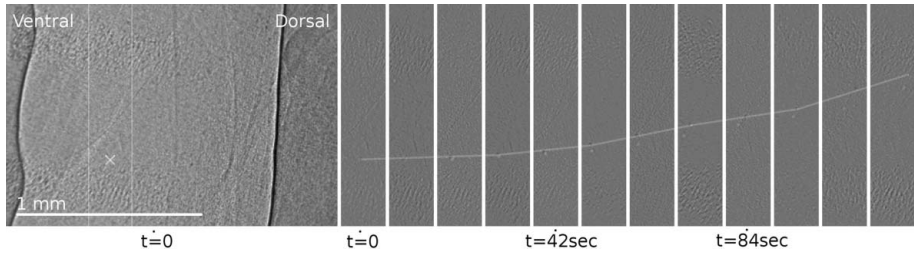

Figure 5
In vivo imaging of quarry dust in a live mouse trachea. The image on the left was captured approximately 1.75 min after imaging was started, and the location of a quarry dust particle is marked with an X. The sequence of image strips to the right (10.5 s apart) were created by cropping complete image frames as marked, to show the same region in subsequent motion-detected frames. The motion of the dust particle is tracked by the grey line, and demonstrates variability in the rate of particle transit for even a single particle. Other particles were also visible when viewed dynamically, but cannot be seen on these static images. Movie S1 in the online supporting information (QuarryDust.avi) contains a time-lapse movie of the *in vivo* behaviour of quarry dust particles.

Independent of the particle type and size, most particle deposition and particle motion occurred on the dorsal region of the trachea. Compared with the number of particulates detected in the 15 µl *in vitro* samples (for example galena in Fig. 2*d*), few particulates were detected *in vivo*. Interestingly, Fig. 4(*b*) shows that galena particulates remained in the ET tube after delivery to the trachea. As we did not normally image at the ET tube site, it is unclear whether this 'trapping' of galena particles in the ET tube was a consistent phenomena.

When particulates were detected they remained visible throughout the entire imaging period. However, most particle motion in the trachea occurred within the first few minutes of imaging, with almost all particles lodging by the end of the imaging period. Small and/or low-density particles continued their motion for longer than large and/or dense particles; the latter were observed to lodge quickly on the airway surface. Almost all galena particulates appeared to be motionless from the initiation of imaging (~1 min after dose delivery), but in comparison some glass beads continued moving for almost the entire imaging period. The motion and lodging of quarry dust and fibreglass were between these two extremes. Quarry dust appeared as compact and irregularly shaped particles. The smallest detectable dust particles were approximately 5 µm in their largest dimension with larger particles up to 20 µm-diameter present. Most dust particles were approximately 10 µm in diameter. Fig. 5 shows a quarry dust particle moving along the airway over a period of 2.1 min.[1] The transit rate of this particle (and many others) was not uniform, and varied between zero and ~0.5 mm min^{-1}. Dust particles were particularly difficult to detect when stationary as they were easily confused with speckled areas of the images, for example regions of bone, cartilage, connective tissue and skin, although motion made these particles more easily detectable.

[1] Supplementary data for this paper are available from the IUCr electronic archives (Reference: MS5027). Services for accessing these data are described at the back of the journal.

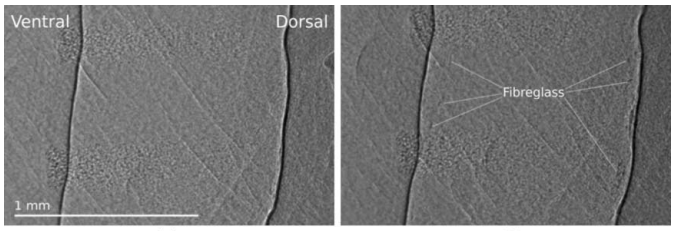

Figure 6
In vivo imaging of fibreglass in a live mouse trachea. (*a*) The trachea immediately prior to fibreglass delivery, and (*b*) the first image captured after imaging began. Although the fibres were visible in the trachea, they did not move throughout the imaging period. Most fibres were located on the dorsal tracheal surface but in this animal a small number were also visible on the ventral surface. Movie S2 in the online supporting information (Fibreglass.avi) contains a time-lapse movie of the *in vivo* behaviour of fibreglass fibres.

Most fibreglass fibres were 10 μm to 15 μm in width, and ranged in length from 30 μm to 80 μm. The relatively long fibre lengths made fibreglass easier to detect *in vivo* than the quarry dust because they were conspicuous against the tissue background. Small approximately spherical fibreglass particles ~10 μm in diameter were also sometimes visible. Fig. 6 shows one example of stationary fibreglass fibres in the trachea. Fibres collected predominantly along the dorsal surface of the trachea, although in this animal a small number of fibres were also present on the ventral surface.

Galena particles did not move substantially over the imaging period, but were easily detected *in vivo* owing to their strong absorption contrast. Particles generally ranged in size from 10 μm up to 25 μm, but clusters of galena approximately 60 μm in diameter were present in two mice. Clusters of this size were not seen in the *in vitro* study (where galena particles were typically less than 25 μm in diameter), suggesting that clustering may have occurred at or after deposition onto the airway surface. In one animal the galena cluster looped between two points in the airway rather than staying stationary; however, this was in contrast to the behaviour of most large galena particles which tended to lodge quickly on the airway surface. Fig. 7 shows the behaviour of this large cluster, with both the transit motion of the galena cluster and the changes in cluster orientation owing to rotation also displayed.

The air contained within the hollow glass beads enhanced their visibility by improving phase contrast, with their spherical shape producing a lensing effect making them visible as relatively bright circles. In the airway the beads were readily visible and varied in size from 10 μm up to ≥20 μm (despite a stated manufacturer's nominal diameter of 14 μm). Fig. 8 shows the motion of multiple glass beads along the dorsal tracheal surface and, like galena, their particle motion was not uniform; beads could move in different directions and at different rates. The transit rate of the marked particles varied between ~0.02 mm min^{-1} distally (toward the lung)

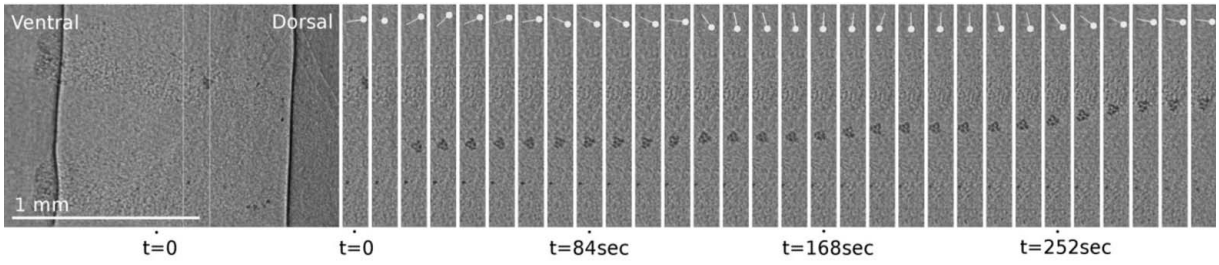

Figure 7
In vivo imaging of galena in a live mouse trachea. The image on the left is the first image captured after imaging began, and shows a large cluster of lead particles, as well as smaller individual particles spread throughout the trachea. The strips on the right (10.5 s apart) show the motion of the lead cluster. The indicator at the top of each strip shows the relative rotation of the cluster. Note that between the first and third strips the cluster movement was briefly retrograde. The majority of the other individual galena particles are located toward the dorsal tracheal wall. Movie S3 in the online supporting information (Galena.avi) contains a time-lapse movie of the *in vivo* behaviour of galena particles.

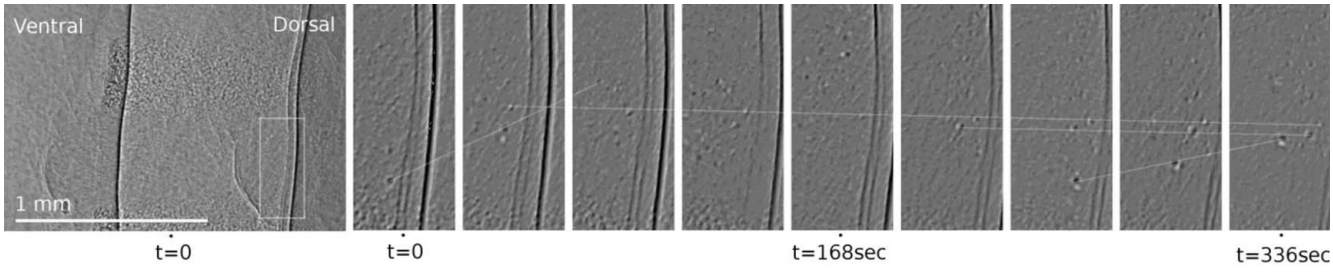

Figure 8
In vivo imaging of silver-coated hollow glass beads in a live mouse trachea. The image on the left was captured approximately 2 min after imaging was started. The strips on the right are motion-detected frames 42 s apart from within the marked white rectangle. The motion of four separate particles is marked: two are moving up the trachea at different speeds, and two are moving more slowly down the trachea. A large number of smaller particles moved faster than these, but are not clear on these static images. The majority of the glass bead particle transit was located toward the dorsal tracheal wall. Movie S4 in the online supporting information (GlassBeads.avi) contains a time-lapse movie of the *in vivo* behaviour of hollow glass beads.

and $\sim$0.37 mm min^{-1} proximally (toward the larynx). In the same animal (data not shown) we also measured smaller glass beads moving proximally at more than twice this rate.

3.3.4. Histological analyses. Histological examination using light microscopy revealed that all the particulate types except asbestos were located on or in the airway epithelium. Samples from mice exposed to quarry dust were inadvertently incorrectly processed and could not be examined. Fig. 9 shows the appearance of the particulates in the trachea under light microscopy. Galena appeared as dense black particles, fibreglass as short green and yellow fibres, and the silver-coated hollow glass beads had a distinctive round shape with a dark edge. We did not identify any asbestos fibres in cross sections from asbestos-treated animals. Particles were located above the airway surface captured in fine mucus strings (visible only in TEM images), embedded within the mucus layer adhering to and overlying the epithelium; and enveloped within the epithelial cells or the epithelial cell ciliary layer. Galena particles were often found more deeply in the epithelial layer than the fibreglass fibres which were typically found at the epithelial cell/air interface, while the glass beads appeared to lodge within and partly displace the cilia and surface liquid of the airway. The spherical glass beads had different apparent diameters and surface detail depending on the level at which they were cut, and small fragments of glass and the silver coating (as verified by EDS analysis) surrounded all of these beads.

EDS analysis was used to confirm the elemental composition of particles present on or in the airway epithelium. Galena produced spectral peaks that corresponded to elements including lead and sulfur; fibreglass to sodium, magnesium, aluminium, silicon and calcium; and the silver-coated glass beads to silicon and silver. The spectra of the particulates present in the trachea sections matched those in the control spectra, confirming the identity of the particles.

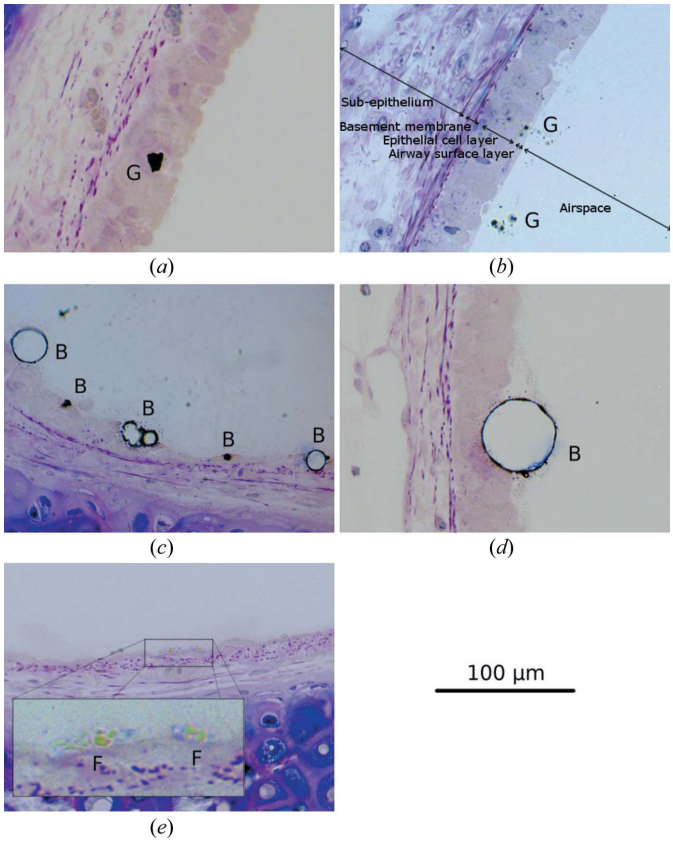

Figure 9
Examples of galena (G), fibreglass (F) and hollow silver-coated glass beads (B), captured on the mouse tracheal airway surface. Tissues were fixed using perfluorocarbon OsO_4, and semi-thin resin sections cut and stained with toluidine blue. Panel (*b*) labels the relevant airway epithelium structures in a typical cross section; note that not all features are present on all panels. (*a*) Galena captured on the surface of the epithelial cell layer, and (*b*) smaller particles within the cell cilia (in the airway surface layer) and embedded in fine mucus strings (not visible here) above the epithelial cells. (*c*) The distinctive glass beads are captured on the airway surface, and (*d*) one large bead of approximately 55 µm diameter appears displaced into the airway epithelium. (*e*) Small fibreglass fibres embedded in the overlying mucus layer.

4. Discussion

The primary goal of this study was to establish methods to deposit a range of common pollutant particles and fibres into live mouse lung airways to enable monitoring of their post-deposition behaviour using synchrotron PCXI. Using histological methods we also sought confirmation of the specific location, and elemental identity, of these particles on or within the cell and surface fluid layers of the airway.

Our *in vivo* results show the suitability of PCXI technology for the detection of particles as diverse as quarry dust, fibreglass, galena and the reference hollow silver-coated glass beads in an intact animal. To our knowledge this is the first report detailing the non-invasive detection and monitoring of the airway surface behaviour of these pollutant particles in live lung airways. This capability is significant because PCXI has the unique ability to image the initial deposition, appearance and movement characteristics of individual pollutant and reference particulates on a live and intact airway surface. The varieties of individual particle behaviour (encompassing consistent speed and direction; stop and start; retrograde movement; changing direction; and rotation behaviour) reveal the diversity in how the airways can handle the deposition and transport of particles. However, the sample size was insufficient to determine whether the different particle types produced distinct patterns of airway surface behaviour. Nevertheless, this new information about the behaviour of individual particles of potential significance in respiratory disease can now supplement well established methods and data derived from monitoring bulk transit rates in airways (Grubb *et al.*, 2004) and can help focus new research into the consequences of particle deposition from the earliest points of their interaction within the airway.

The *ex vivo* pilot study demonstrated that the particulates could easily be detected in an excised trachea with little loss of the identifying characteristics present in our *in vitro* studies.

We suspect that the visible tissue dehydration was caused by the dry air within the imaging hutch, and was further exacerbated by repeated exposures to the intense X-ray beam. With fluid bathing, reliable and precise temperature control, heat dissipation and physiological support we expect that tissue viability would be maintained and dehydration would be eliminated. Since this pilot was only intended to examine the visibility of the tissue and particulates and to demonstrate the feasibility of performing an *ex vivo* study, we did not use it to examine the deposition and clearance behaviour of the test particulates. Comparison with the *in vivo* images confirmed that the tissue surrounding the trachea was the source of background detail that could obscure some particles in captured images. The absence of surrounding tissues, as well as respiratory and cardiac movements, substantially improved particulate visualization in the *ex vivo* system, particularly for those particulates that lodged on the airway surface. We propose that trials in a functional *ex vivo* system may provide a rapid and accurate method to estimate baseline transit rates prior to testing *in vivo*, although the absence of reciprocating airflows may alter airway surface clearance behaviour, as flows are known to affect epithelial cell physiology (Tarran *et al.*, 2005).

In earlier studies of mouse nasal airways (Donnelley *et al.*, 2009) we determined that a 15 µl delivered dose was sufficient, but a particle/fibre concentration of 0.1% *w*/*v* used there did not provide an adequate number of particles to detect and analyse transit behaviour. Not surprisingly, compared with that nasal study the ten-fold higher particle concentration (1% *w*/*v*) used here resulted in many more deposited particulates, although still less than expected based on the *in vitro* results. This difference could be explained by the different delivery set-ups: a pipette for the *in vitro* study and a long cannula and glass syringe for the *in vivo* study. Interestingly, we noted there were many particulates visible in the ET tube (*e.g.* Fig. 4*b*) suggesting that the effectiveness of the delivery system was not optimal. The cannula material may have adherent properties for these particles, so delivery may be improved by using different cannula materials or surface coatings, altering the particulate delivery rate, or adjusting the volume and rate of ET airflow. In addition, unlike in the nasal study we did not detect asbestos fibres *in vivo* using PCXI, nor in sections examined under light microscopy or TEM. In bench studies we have noted that asbestos fibres are prone to clustering and blockage of fine delivery cannulae, so we speculate that asbestos was not successfully delivered to the trachea. In future studies we will refine our techniques and set-up to ensure correct asbestos delivery.

The behaviour of fibreglass fibres in the trachea differed from that noted in earlier nasal airway studies (Donnelley *et al.*, 2009). In the trachea, individual fibreglass fibres were observed, whilst in the nasal airway study fibres were only present within a liquid envelope and individual fibres were not visible. This finding indicates that particle behaviour may be determined by the deposition location within the respiratory system. This may not be surprising, since the nose has evolved to trap particles after inhalation to prevent their inhalation into the conducting airways and lungs. We also noted that particle behaviour in the trachea was determined by both the type and size of the particles. Smaller and/or low-density particles tended to move faster and for longer periods, and we speculate this was because these particles take longer to be captured on the epithelial surface or in mucus on and above the surface. Regardless of the type or size of the particles, individual particle behaviour was often extremely variable. Thus, while it was possible to visualize individual particle behaviour, this technique does not measure bulk particle transit rates. Despite the vertical orientation of the animal the transit of all particles was consistently localized to the dorsal tracheal wall.

Histological analysis showed that galena particles and glass beads could displace cilia and surface liquid and lodge within the surface of the airway epithelium. Such a behaviour has been predicted for small particles elsewhere (Gehr & Schurch, 1992) and may be related to the surface tension forces acting on the particles. This effect may also be independent of the presence of airway surface mucus. Such a non-specific process might help explain why we observed that so many particles ceased moving soon after delivery.

There were several limitations in this study. Although our PCXI set-up can resolve particles down to less than 4 µm, the visual complexity produced by the anatomical structures surrounding a moving trachea in a live animal means that particles of approximately 5 µm diameter are currently the smallest particles we can accurately detect and track. This is close to the upper size limit for particles that can reach and deposit in the human trachea after inhalation (Oberdorster *et al.*, 2005). Despite this limitation, PCXI was demonstrated to be suitable for examining particulate deposition and post-deposition behaviour, and with improvements in technology the visualization of smaller particles will be possible in the near future.

Both Nembutal (King *et al.*, 1979) and isoflurane (Robertson *et al.*, 2004) have been reported to alter mucociliary transit by affecting mucus rheology and ciliary beat frequency. Therefore it is likely that the true rate of transit is faster than the results suggest. However, the ciliary beat pattern has been shown to be unaffected by isoflurane anaesthesia (Robertson *et al.*, 2004). We are limited by Japanese Government regulation in the choice of anaesthetics available for experiments at the SPring-8 synchrotron, but it is apparent that across the different particle and fibre types, all delivered under the same anaesthetic regime, there are clear differences in post-deposition transit behaviour.

This study was also constrained by the inability to enter the synchrotron imaging hutch during imaging. In these first experiments the ventilator was integrated into the imaging set-up in a manner that required manual particulate instillations to be performed. This necessarily introduced a delay while the beamline hutch door was closed and the X-ray shutter was opened to begin imaging, so it was not possible to visualize the actual instillation of the particulates into the mouse airway. Accordingly, we could not observe the presence and clearance of the initial bulk-liquid dose, and our first live images (albeit

performed within 1 min of instillation) sometimes revealed that particles had already lodged on the airway surface. Owing to this delay it was also impossible to assess whether any particles in the initial 15 µl bolus were carried directly down toward the lungs. However, the absence of bulk dose fluid on the airway surfaces immediately after dosing (when imaging began) suggests there was a very rapid loss of the dose vehicle, leaving the pollutants deposited on the airway surface. It also suggests that delivering the pollutants within a liquid carrier rather than as dry particles or fibres may have little persistent effect on the airway environment or the deposition behaviour. The experimental complexity and the occupational hazards to researchers when delivering dry or aerosolized pollutant particles are difficult to handle; however, these studies have provided encouraging data to support the efforts needed to safely and effectively test these more physiologically normal delivery methods in the future.

Owing to image complexity from the mouse anatomy and motion from respiratory movements we limited the analysis to the trachea rather than examining the intrapulmonary airways. In future studies we plan to modify the delivery and imaging set-up to enable particulate delivery during imaging to capture the first interactions of the pollutants with the airways and to examine the deeper lung airways where particulate deposition is also important.

Although we limited the radiation dose by reducing the size of the imaging area and minimizing the exposure times, at present the dose delivered using this experimental set-up is too large to consider animal recovery or repeat-imaging experimental designs. However, in other experiments we have found that the exposure times and dose can be reduced by at least a factor of three by increasing the thickness of the scintillator and using a higher quality objective lens. In addition, depending on the experimental aims the number of exposures can be substantially reduced and image quality may be traded for further reductions in exposure length and dose. In addition, the rapid development of imaging and synchrotron technologies should also produce improvements in light sensitivity and image resolution that could allow shorter exposure times to minimize motion artefact and produce desired reductions in radiation dose. With these improvements we expect the dose could realistically be reduced by a factor of ten compared with that delivered in this experiment. Our goal remains to progressively improve our maximum resolution, allowing smaller and therefore more physiologically relevant particulates to be detected and tracked.

Despite these limitations and challenges there are currently no alternative *in vivo* imaging modalities able to non-invasively detect and track such small individual particles or fibre clusters in the mouse *trachea*. Thus we propose that PCXI is a valuable technique for studying the deposition and behaviour of pollutant particles and fibres in the airways of live animal models. We also expect that these experimental techniques will be useful for other synchrotron experiments imaging the upper lung airways of small animals, and are a practical addition to the range of related techniques we have established for use in mouse *nasal* airways.

5. Supplementary files

The four supplementary files contain movie sequences showing particulate and fibre behaviour on the tracheal airway surface, and are the source of the images shown in Figs. 5–8. Each 10 s time-lapse video shows 3.5 min of baseline image collection (20 images, 10.5 s apart), followed by 14 min of post-deposition imaging (80 images, 10.5 s apart), and are presented at 105× normal speed. Between the acquisition of these two sequences the particulates were manually delivered into the trachea. All videos are avi files, were encoded using the *DivX* codec and can be played using the free VLC Media Player (available at http://www.videolan.org/vlc/).

These studies were supported by the WCH Foundation, NH&MRC Australia, USA CF Foundation and philanthropic donors *via* the CURE4CF Foundation (http://www.cure4cf.org/). The synchrotron radiation experiments were performed on the BL20XU beamline at SPring-8, with the approval of the Japan Synchrotron Radiation Institute (JASRI) under proposal number 2009A1878. Dr Andreas Fouras, Monash University Division of Biological Engineering, provided imaging advice and supplied essential experimental equipment including the CCD detector. Mr Paul Whiffen, Environment Manager, Boral Resources (SA) Limited, provided dolomite quarry dust samples. Ruth-Ellen Williams performed the histological preparation and assisted with TEM and EDS at Adelaide Microscopy, and Richard Bright performed the light microscopy and sample preparation at the Women's and Children's Hospital. KSM was supported by an Australian Postgraduate Award, a Monash University J. L. William Scholarship and a Cystic Fibrosis Australia Studentship. MD, KSM, KKWS and DWP were supported by the AMRF Program, Commonwealth of Australia.

References

Cloetens, P., Barrett, R., Baruchel, J., Guigay, J. P. & Schlenker, M. (1996). *J. Phys. D*, **29**, 133–146.
Donaldson, S. H., Corcoran, T. E., Laube, B. L. & Bennett, W. D. (2007). *Proc. Am. Thorac. Soc.* **4**, 399–405.
Donnelley, M., Morgan, K. S., Fouras, A., Skinner, W., Uesugi, K., Yagi, N., Siu, K. K. W. & Parsons, D. W. (2009). *J. Synchrotron Rad.* **16**, 553–561.
Gehr, P. & Schurch, S. (1992). *News Physiol. Sci.* **7**, 1–5.
Goss, C. H., Newsom, S. A., Schildcrout, J. S., Sheppard, L. & Kaufman, J. D. (2004). *Am. J. Respir. Crit. Care Med.* **169**, 816–821.
Grubb, B. R., Jones, J. H. & Boucher, R. C. (2004). *Am. J. Physiol. Lung Cell Mol. Physiol.* **286**, L588–L595.
Hamacher, J., Arras, M., Bootz, F., Weiss, M., Schramm, R. & Moehrlen, U. (2008). *Lab. Animals*, **42**, 222–230.
King, M., Engel, L. A. & Macklem, P. T. (1979). *J. Appl. Physiol.* **46**, 504–509.
Limberis, M., Anson, D. S., Fuller, M. & Parsons, D. W. (2002). *Human Gene Therap.* **13**, 2112.
Livraghi, A. & Randell, S. H. (2007). *Toxicol. Pathol.* **35**, 116–129.
Oberdorster, G., Oberdorster, E. & Oberdorster, J. (2005). *Environ. Health Perspect.* **113**, 823–839.
O'Connor, G. T., Neas, L., Vaughn, B., Kattan, M., Mitchell, H., Crain, E. F., Evans, R., Gruchalla, R., Morgan, W., Stout, J., Adams, G. K.

& Lippmann, M. (2008). *J. Allergy Clin. Immunol.* **121**, 1133–1139.
Parsons, D. W., Morgan, K., Donnelley, M., Fouras, A., Crosbie, J., Williams, I., Boucher, R. C., Uesugi, K., Yagi, N. & Siu, K. K. W. (2008). *J. Anat.* **213**, 217–227.
Robertson, A., Stannard, W., Passant, C., O'Callaghan, C. & Banerjee, A. (2004). *Clin. Otolaryngol.* **29**, 157–160.
Sims, D. E., Westfall, J. A., Kiorpes, A. L. & Horne, M. M. (1991). *Biotech. Histochem.* **66**, 173–180.
Siu, K. K. W., Morgan, K. S., Paganin, D. M., Boucher, R., Uesugi, K., Yagi, N. & Parsons, D. W. (2008). *Eur. J. Radiol.* **68**, S22–S26.
Snigirev, A., Snigireva, I., Kohn, V., Kuznetsov, S. & Schelokov, I. (1995). *Rev. Sci. Instrum.* **66**, 5486–5492.
Stocker, A., Kremer, K., Koldej, R., Miller, D., Anson, D. & Parsons, D. (2009). *J. Gene Med.* **11**, 861–867.
Tarran, R., Button, B., Picher, M., Paradiso, A. M., Ribeiro, C. M., Lazarowski, E. R., Zhang, L. Q., Collins, P. L., Pickles, R. J., Fredberg, J. J. & Boucher, R. C. (2005). *J. Biol. Chem.* **280**, 35751–35759.
Wildhaber, J. H. (2006). *Paediatr. Respir. Rev.* **7**(Suppl. 1), S86–S87.
Wilkins, S. W., Gureyev, T. E., Gao, D., Pogany, A. & Stevenson, A. W. (1996). *Nature (London)*, **384**, 335–338.
Yabashi, M., Yamazaki, H., Tamasaku, K., Goto, S., Takeshita, K., Mochizuki, T., Yoneda, Y., Furukawa, Y. & Ishikawa, T. (1999). *Proc. SPIE*, **3773**, 2–13.